

Numerical Analysis and Optimization of Die Compaction Process

Young-Sam Kwon and Suk-Hwan Chung
CetaTech, Inc.

TIC, 296-3, Seonjin-ri, Yonghyeon-myon, Sacheon, Kyongnam, 664-953, Korea

Howard I. Sanderow
Management & Engineering Technologies
161 Copperfield Drive, Dayton, OH 45415, USA

KiTae Kim
Department of Mechanical Engineering, Pohang University of Science and Technology (POSTECH),
San 31, Hyoja-Dong, Nam-Gu, Pohang 790-784, Korea

Randall M. German
Center for Innovative Sintered Products, P/M Lab, 147 Research West
The Pennsylvania State University, University Park, PA 16802-6809, USA

ABSTRACT

The optimization program (PMSolver) is developed to analyze and optimize the powder compaction. The optimization program has the capability to predict (1) the formation of cracks in the green compact, (2) the density distribution in the compact and (3) the tooling forces required to achieve these densities and (4) provide the optimum processing variables during powder compaction.

The optimization program is applied to predict the density distribution and tooling forces. Based on the verification of the program, loading schedule is optimized to achieve uniform density distribution in the Hub shaped green part during die compaction. This part had been previously analyzed by several compaction simulation models through the European consortium MODNET. A new concept to predict crack formation during powder compaction is proposed. The numerical simulation results show excellent agreement with experimental data and the process conditions obtained by the optimization procedure remarkably improve the quality of product.

INTRODUCTION

The die compaction of metal and ceramic powders is a conventional powder consolidation method for the production of net-shaped components [1]. The trend of industry to enhance the productivity and reliability is to reduce the number of total components and increase the mechanical properties. To meet this trend, high performance and complex P/M parts have to be developed, where it is possible by increasing density and uniformity. Also, the computer numerical control (CNC) compaction press with multi actuator can manufacture more complicated P/M components.

During die compaction, the friction between a powder body and tooling surface and non-uniform stress from tools along the tool-contacted surface of a powder body are inevitable and cause non-uniform density distribution in a powder compact [2]. Non-uniform density distribution is a serious problem in the reliability and performance of P/M part and the net-shape forming, since the heterogeneities can generate cracks during die compaction and contribute to non-uniform shrinkage during sintering. The proper

selection of the process parameters such as die shape, upper and lower punch displacements, and sequential tool motions helps eliminate the heterogeneities. Up to now the compaction parameters were guess-estimated based on engineer's experience. However, the move toward more complicated components require more complex die and punch systems.

The European consortium PM MODNET [2] compared the computer models for the numerical simulation of powder compaction with the experimental data of density and tooling forces during die compaction for an axisymmetric hub shaped part with an atomized iron-based powder. They used Cam-Clay model and Drucker-Prager-cap model as the computer models. The numerical simulation with Drucker-Prager-cap model showed better performance in the prediction of density, while Cam-Clay model showed better performance in the prediction of tooling force. However, the mechanism and criteria for crack prediction were not well understood with their simulation work.

Die compaction experiments for an axisymmetric hub shaped part were performed by a hydraulic press with multi actuator [3]. The tooling equipment consists of the upper punch, the lower outer punch, the lower inner punch and die. Even though the lower outer punch was the fixed component, three process parameters such as the upper punch, the lower inner punch and die have to be controlled. They used five different conditions for the upper punch, the lower inner punch and die. But, there can be a number of processing conditions since the three independent process parameters make many combinations. Recently, Kwon et al. developed the optimization program (PMSolver) to provide the optimum process conditions to achieve the most uniform density distribution inside the powder compact [4].

In this paper, we use Shima and Oyane model [5] for the simulation of die compaction and propose a simple method to determine the material parameters for Shima and Oyane model. The numerical simulation of the density distribution and tooling forces for the same experiments with PM MODNET is verified by comparing it with experimental data [3]. Also, a new concept for the crack formation during die compaction is proposed to predict crack formation. Finally, the process parameters are optimized to obtain uniform density distribution by using the optimization tool, PMSolver [4].

ANALYSIS OF DIE COMPACTION PROCESS

Constitutive model

In die compaction, the deformation behavior of the powder body is based on the yield criterion. Unlike bulk solids, the yield criterion includes the hydrostatic pressure due to volume change in compaction. Among many yield criteria for compaction [6], Shima and Oyane's criteria [5] is of the form

$$\Phi = \left(\frac{q}{\sigma_m} \right)^2 + 6.20(1-D)^{1.028} \left(\frac{p}{\sigma_m} \right)^2 - D^5 \quad (1)$$

Where, q and p are the effective stress and hydrostatic pressure, D is the relative density, and σ_m is the flow stress of matrix material. Many researchers used Eq. (1) to analyze the compaction process with various powder materials and Eq. (1) has been successfully applied to die compaction process with stainless steel powder [7]. But, Eq. (1) was derived from the uniaxial compression and tension experiments with copper powder from the following generalized yield criteria:

$$\Phi = \left(\frac{q}{\sigma_m} \right)^2 + \alpha(1-D)^\gamma \left(\frac{p}{\sigma_m} \right)^2 - D^m \quad (2)$$

where α , γ and m are the material parameters. So, Eq. (1) is the yield function for only copper powder and new material parameters in Eq. (2) have to determine for other powder materials.

Determination of Material Parameters

In this paper, we used the generalized Shima and Oyane model, Eq. (2). Shima and Oyane determined the material parameters α and γ by fitting the axial and radial strain data from uniaxial compression tests with various relative density samples. Also, the material parameter n was determined by fitting the yield stress data from uniaxial compression and tension tests with various density samples.

The procedure of the material parameters determination by Shima and Oyane requires only uniaxial stress state data (uniaxial compression and tension tests). But, die compaction process is performed at a higher triaxial stress state than uniaxial stress state. The values of yield stress with various densities showed the large scattering at the tensile and compression test [5] and the determination of the material parameter n is not accurate. Even though the material parameter n can be determined by fitting the yield stress data, the die compaction process of metal powder is fully plastic deformation process. To determine the reasonable material parameters for Shima and Oyane model, triaxial test data have to be used.

To complete the yield function, Eq. (2), the flow stress of matrix material σ_m has to be measured. In the numerical simulation, the flow stress of matrix material σ_m is very important value to predict the tooling force. The flow stress of matrix material σ_m can be considered the material constant and found from material handbook. But, the flow stress of matrix material σ_m depends on the composition, processing condition, grain size and so on. To obtain the accurate flow stress of matrix material, uniaxial compression test were performed with a bulk sample prepared by hot isostatic pressing of the same powder material [7].

The friction between the powder and tooling surface can be considered by using the proper friction coefficient. The friction coefficient μ depends on the particle size, hardness, roughness of tool, amount of lubricant and so on. There are many efforts to measure the friction coefficient and Kwon et al.[7] used the ejection force with applied pressure to measure the friction coefficient. The measurement of the friction coefficient is still an important research issue.

The complicated procedure to determine the material parameters including the flow stress of matrix material σ_m and the friction coefficient μ has obstructed the practical use of the numerical simulation in the process and tooling system design. In this paper, we tried to find the material parameters, α , γ , m , σ_m and friction coefficient μ from the simple die compaction test. We assumed the following expression for the flow stress of matrix material σ_m :

$$\sigma_m = a + b\bar{\epsilon}_m^n \quad (3)$$

where, a , b and n are the material parameters and $\bar{\epsilon}_m$ is the effective strain of matrix material.

Damage Model

In die compaction process, crack formation during compaction and ejection is very important problem. Coube used the Drucker-Prager-cap model and Drucker-Prager failure surface to explain the crack formation [8]. The Drucker-Prager failure surface has the empirical background to explain the crack formation. But, the numerical simulation for the crack formation cannot provide the decision whether a crack generates or not because there is no accurate criteria to predict crack formation.

In this paper, we used Shima and Oyane yield model and Drucker-Prager failure surface for the crack formation. Shima and Oyane model is elliptical shape in the stress space as shown in Figure 1. A new concept for crack formation, failure separation length (FSL), can be considered. FSL means the accumulated separation length from Drucker-Prager Failure Surface as shown in Figure 1. During the numerical simulation of die compaction process, we can investigate the stress path of all elements and we

can check whether a specific region go over the Drucker-Prager failure surface. The accumulated separation length from Drucker-Prager Failure Surface can show the possibility of crack formation.

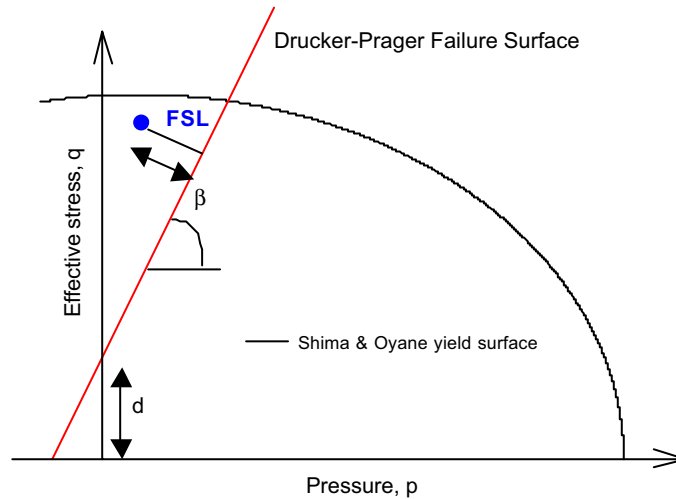


Figure 1. Definition of failure separation length (FSL) based on Shima and Oyane yield model and Drucker-Prager Failure Surface

Optimization Scheme

In using a derivative based optimization scheme, it is important to define searching direction and stepping size. In this study, the searching direction is decided by the conjugate gradient method and the stepping size is decided by the polynomial curve fitting. In deciding the stepping size, two additional finite simulations are necessary, since the polynomial curve fitting needs three objective function values [4].

Figure 2 shows the flow chart of the optimization scheme used in this paper. First of all, a process designer should choose the proper initial guess for loading schedule. Using the results of finite element simulation with mesh system generated by the given loading schedule, design sensitivities are calculated by the adjoint variable method. And then, the searching direction is decided by the conjugate gradient method and the proper stepping size is decided by the polynomial curve fitting with the objective functions obtained by additional finite element simulations. The design parameters are iteratively updated until the convergence criteria are satisfied.

EXPERIMENTS

Simple Die compaction Test

Atomized iron-based powder (Distaloy AE, Höganäs) was used in this work. Its chemical composition is shown in Table 1.

Die compaction response of the iron-based powder was investigated in a closed die under single action pressing. Die compaction tests were performed with two different methods to get the pressure-density response of the iron-based powder without and with friction effect. To investigate the relation between the relative density and pressure of the iron-based powder without the friction effect, graphite-type lubricant was applied on the die wall and small amount powder (4.5 g) was poured in a closed die with 11.28 mm in diameter. The die was made of cemented carbide. The iron-based powder was compacted under axial pressure from 50 to 500 MPa.

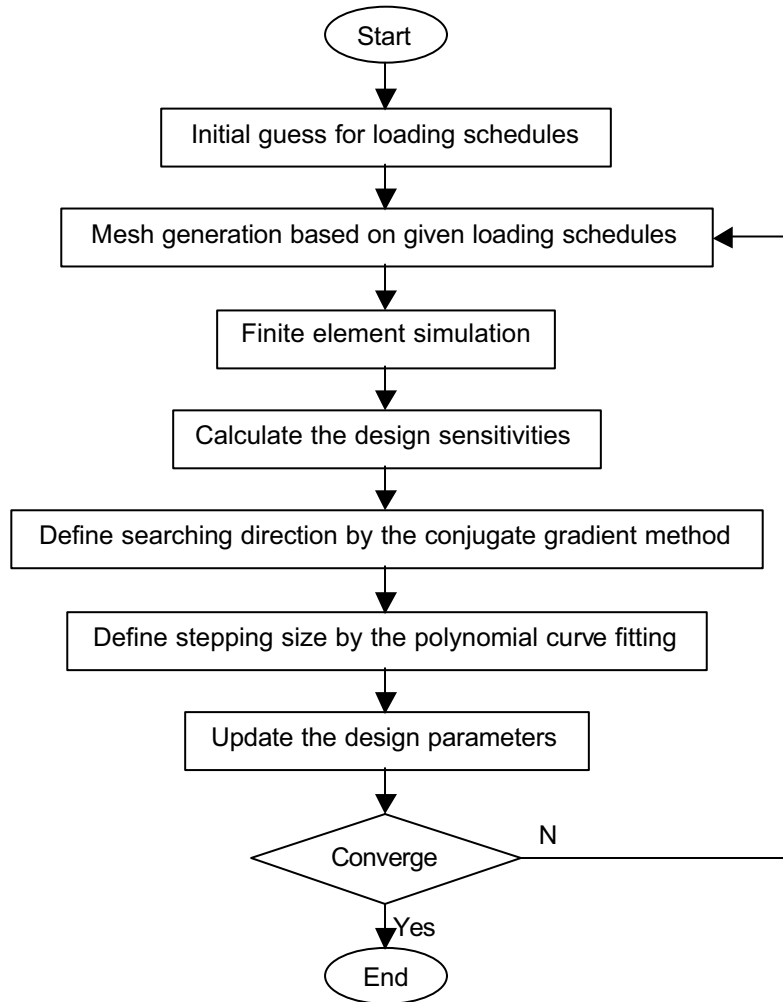


Figure 2. Flow chart of optimization scheme

Table 1. Chemical composition of iron-based powder used in this work

(wt%)	Ni	Cu	Mo	C	Wax	Fe
Distaloy AE	4.2	1.5	0.5	0.5	1.0	bal.

Also, to investigate the relation between the relative density and pressure of the iron-based powder without the friction effect, lubricant wasn't applied on the die wall and a little more powder (9.3 g) was poured in a closed die with 11.28 mm in diameter. The iron-based powder was compacted under axial pressure from 50 to 500 MPa.

Determination of Material Parameters

In this work, we used the same material parameters α and γ that Shima and Oyane used for the iron-based powder as follows:

$$\alpha = 6.20, \gamma = 1.028. \quad (4)$$

The material parameter m and the flow stress of matrix material σ_m were obtained by minimizing the difference between the calculation and the measured variation of relative density with pressure during the die compaction process without friction effect. The material parameter m and the flow stress of matrix material were determined as follows:

$$m = 7.4, \sigma_m = 184 + 200\bar{\epsilon}_m^{0.24} \text{ (MPa)}. \quad (5)$$

The friction coefficient $\mu = 0.1$ was obtained by minimizing the difference between the finite element simulation results with the determined material parameters in Eqs. (4) and (5) and the measured variation of relative density with pressure during the die compaction process with friction. Figure 3 shows the variation of relative density with pressure for the iron-based powder during die compaction.

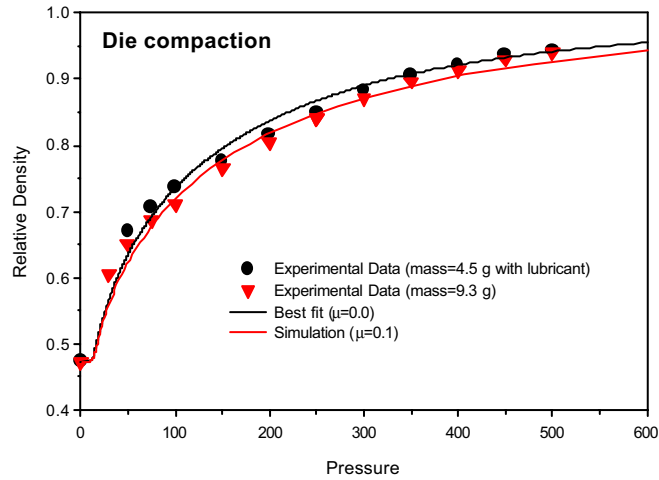


Figure 3. Variation of relative density with pressure for the iron-based powder during die compaction

RESULTS AND DISCUSSION

Finite Element Analysis

To verify the finite element results the process conditions of Part 9 and Part 34 in reference [3] are chosen, where the density distribution and crack formation of several process conditions were compared. The compaction tool set consists of upper punch (P1), lower outer punch (P2), lower inner punch (P3), core rod, and die as shown in Figure 4. Figure 5 shows the loading schedules of punches and dies.

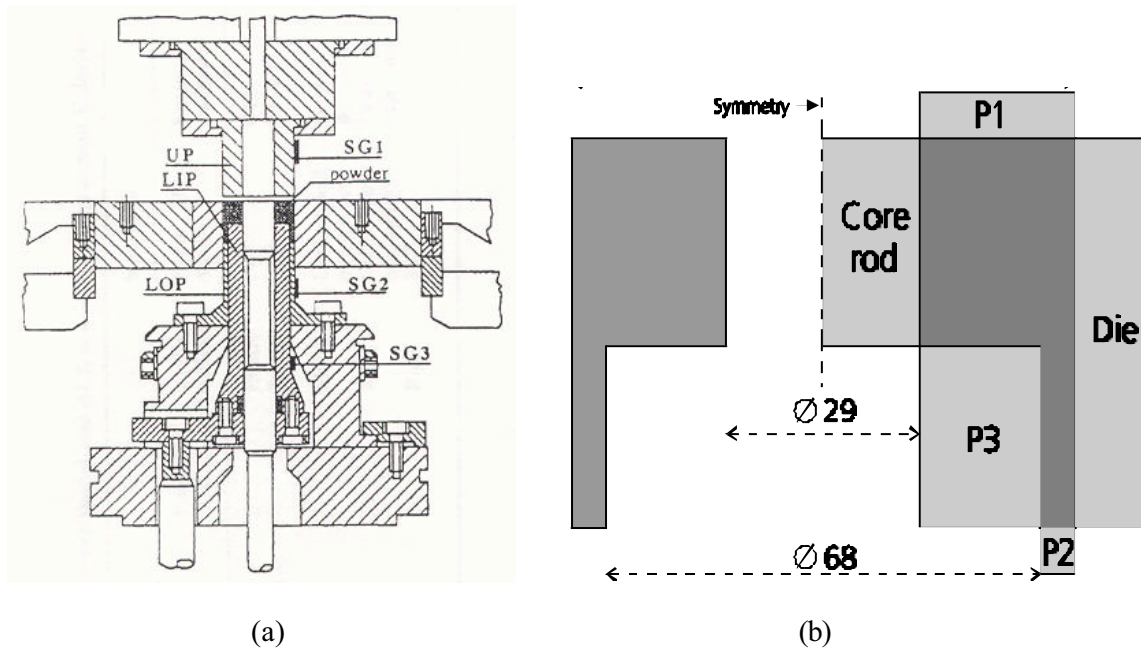


Figure 4. Configuration of compaction tool set and geometry of the part [3]

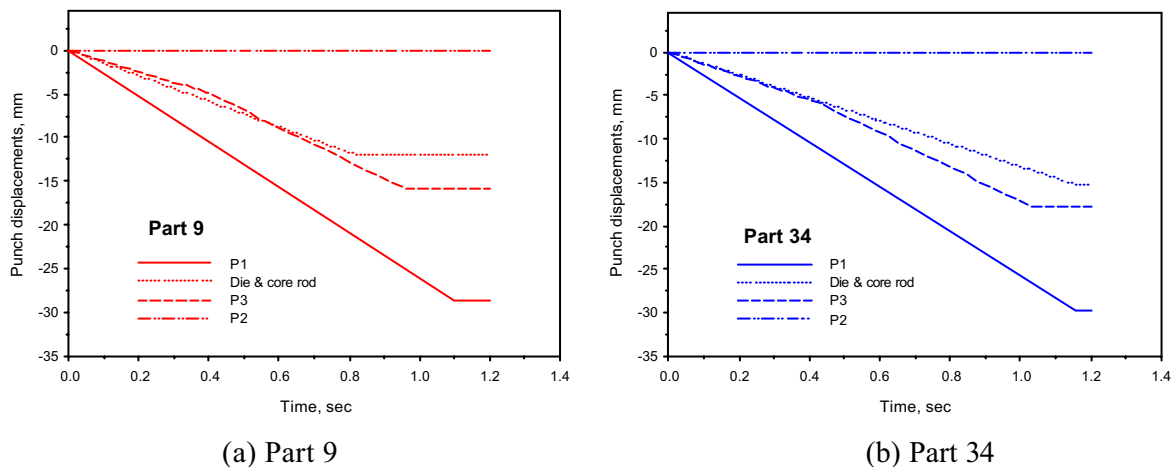


Figure 5. Loading schedules of compaction tool sets

The solid density is 7.33 g/cm^3 and the initial density is 3.47 g/cm^3 , that is, the initial relative density is 0.47 [3]. Numerical simulation was performed using the die compaction process analysis program, PMSolver/compaction-2D with the determined material parameters, the flow stress of matrix material and

the friction coefficient [4].

Figure 6 shows the comparison the density distribution at the end of compression by numerical simulation for Part 9 and Part 34 loading schedules. Considering the result of the loading schedule of Part 9, density in the lower region is higher than in the upper region. Therefore, it is needed to adjust the loading schedule so as to reduce the difference in density. In contrast, in the case of part 34, density in upper region is higher than in lower region. The difference between the highest density region and lowest density region in part 34 is smaller than in part 9. This means Part 34 has more uniform density distribution than Part 9 and the loading schedule of Part 34 is better than that of Part 9.

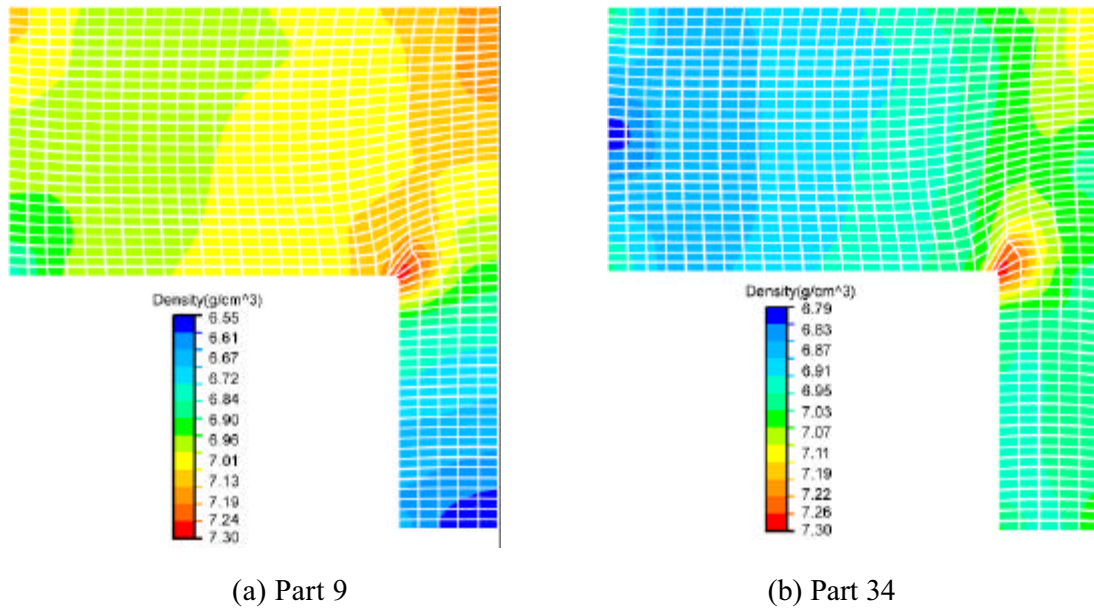


Figure 6. Comparison of density distribution at the end of compression for (a) Part 9 and (b) Part 34 loading schedules

The density distribution at the end of compression by numerical simulation was compared with the experimental results. Figure 7 shows the sections where densities were measured after cutting the part into 5 sections [3].

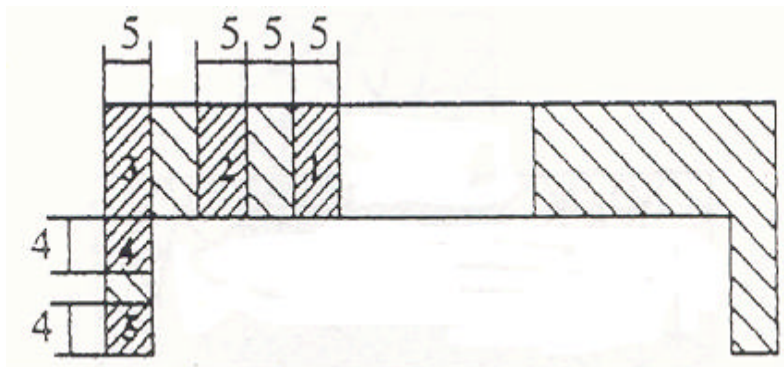


Figure 7. Density distribution measurements [3]

Table 2 shows the comparison of densities between simulation results and experiment in Part 9 and Part 34. The finite element simulation results are in very excellent accordance with experimental results. The prediction of density is within 0.05 g/cm^3 except three cases.

Table 2. Comparison of densities between experimental data and simulation results in Part 9 and Part34 (unit : g/cm^3)

Block	Part 9			Part 34		
	Experiment	Model	Experiment - numerical	Experiment	Model	Experiment - numerical
1	6.97	6.99	-0.02	6.90	6.89	0.01
2	7.02	7.02	0	6.93	6.94	-0.01
3	7.04	7.09	-0.05	7.03	7.07	-0.04
4	6.83	6.89	-0.06	6.91	7.03	-0.12
5	6.78	6.64	0.14	6.97	7.00	-0.03

In most forming processes, die force has been a representative target with which the numerical simulation result has been verified. Numerical simulation results were compared with experiment data of die forces of punches, core rod and die as shown in Figure 8. Die forces obtained by numerical simulation were in excellent accordance with experimental data, where the results show that die forces of Part 34 were lower than those of Part 9.

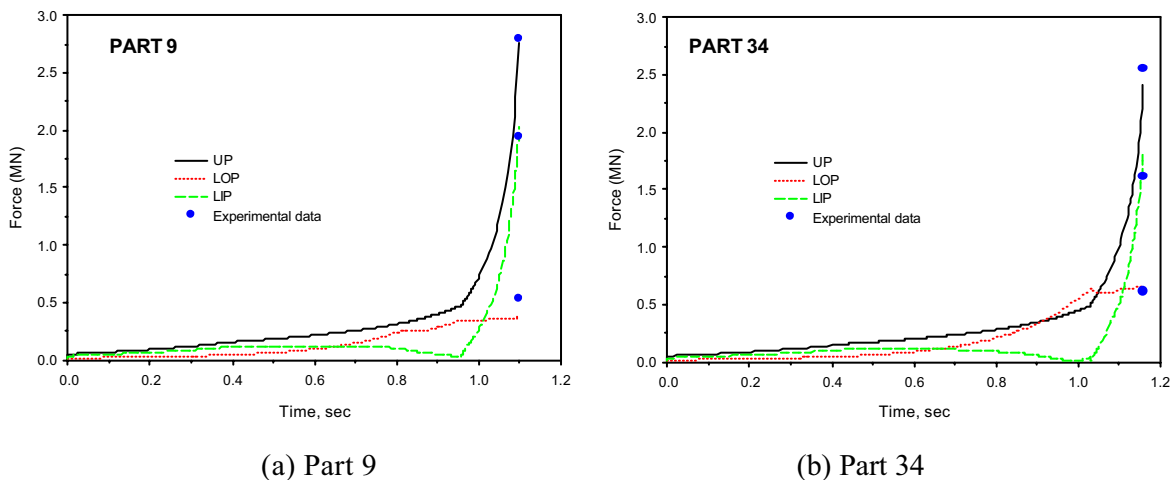


Figure 8. Comparison between experimental data and numerical simulation results for variation of die forces with time for (a) Part 9 and (b) Part 34 loading schedules

Table 3 shows the comparison of tooling forces between simulation results and experimental data in Part 9 and Part 34. The finite element simulation results are in reasonably good accordance with experimental data. The prediction of tooling forces is within 15% except only one case.

To be useful, the simulation needs to be accurate in the prediction of density within 0.1 g/cm^3 and tooling force within 20% [2]. The simulation results with Shima and Oyane model and the material parameters by

very simple experiments are very accurate and useful.

In Figure 6, the density is very high at the junction between the rim and hub. This means that locally concentrated deformation may invoke high possibility of crack formation. Using the proposed concept for crack formation, the interrelation between failure separation line (FSL) and crack formation in real phenomena was verified. Figure 9 shows the comparison of FSL between Part 9 and Part 34, where Part 34 shows relatively small magnitude of FSL. This shows that the possibility of crack formation in Part 9 is higher than in Part 34. Considering the results of reference [3], crack was observed in Part 9 but in Part 34 no apparent defect was observed. This result shows that the proposed FSL can quantify the amount of crack formation.

Table 3. Comparison of tooling force between experiment and simulation in Part 9 and Part34

Tools	Part 9			Part 34		
	Experiment	Model	% Error of Model	Experiment	Model	% Error of Model
UP	2.79	2.76	1.3	2.55	2.41	5.4
LIP	1.94	2.03	4.8	1.61	1.83	12.1
LOP	0.53	0.38	28.8	0.61	0.69	14.5

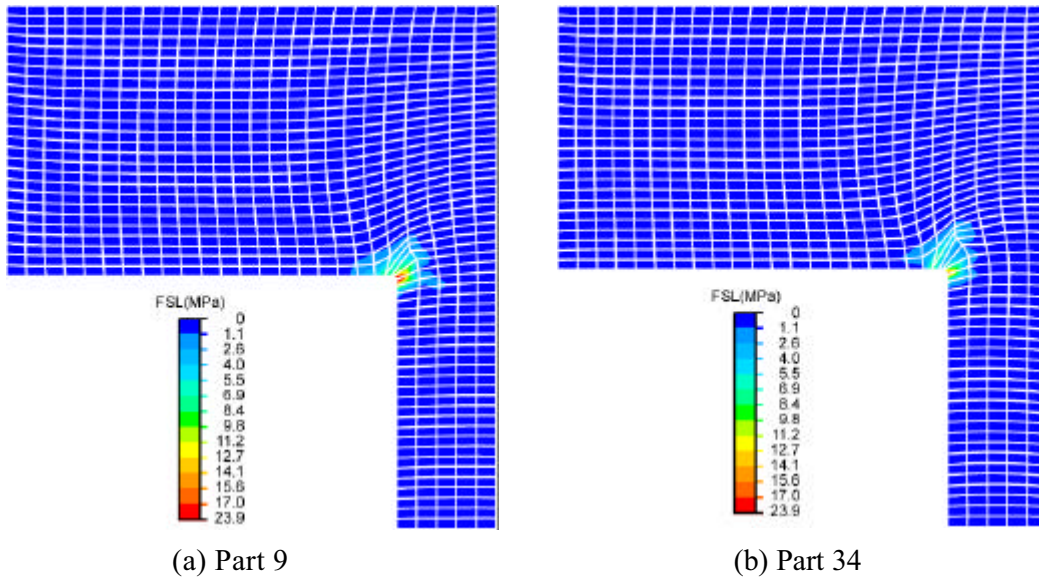


Figure 9 Comparison of failure separation length (FSL) between Part 9 and Part 34

Optimization of Loading Schedule

To obtain more uniform density distribution than Part 34, optimization technique presented in Figure 2 was applied. The objective function was the deviation of relative density. The design parameters were the positions of each punch, rod, and die, where time division was kept as shown in Figure 4(b). Lower outer punch (P2) was kept stationary and the initial position of lower inner punch (P3) was determined so that total initial volume should be conserved. And the movement of core rod and die was synchronized. The final positions of all punches and dies were conserved, since the final shape had been already determined. Therefore, the active design parameters in this case were the initial position of upper punch, initial position of core rod and die, and the second position of lower inner punch (P3) at $t = 0.43$ sec.

Figure 10 shows the variation of objective function during the optimization iteration. Figure 11 shows the comparison of loading schedules between optimal case and Part 34. Through the optimization iteration, the optimal loading condition revealed to locate remarkably apart from the loading condition of Part 34.

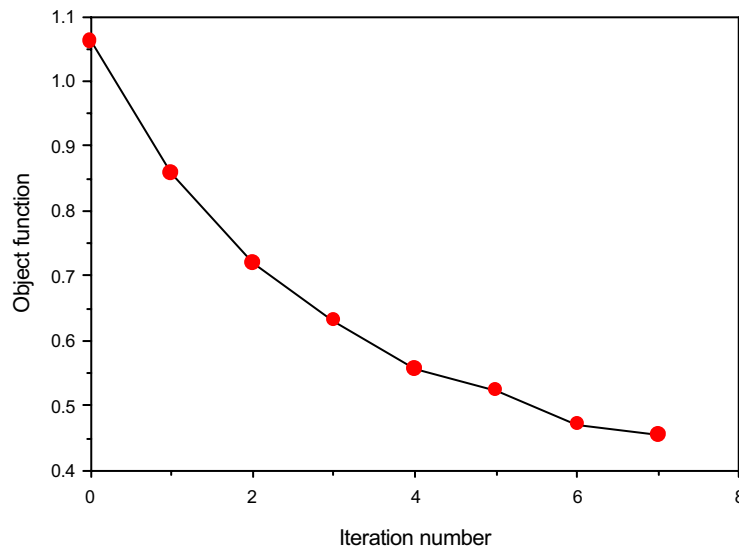


Figure 10. Variation of the object function during optimization iteration

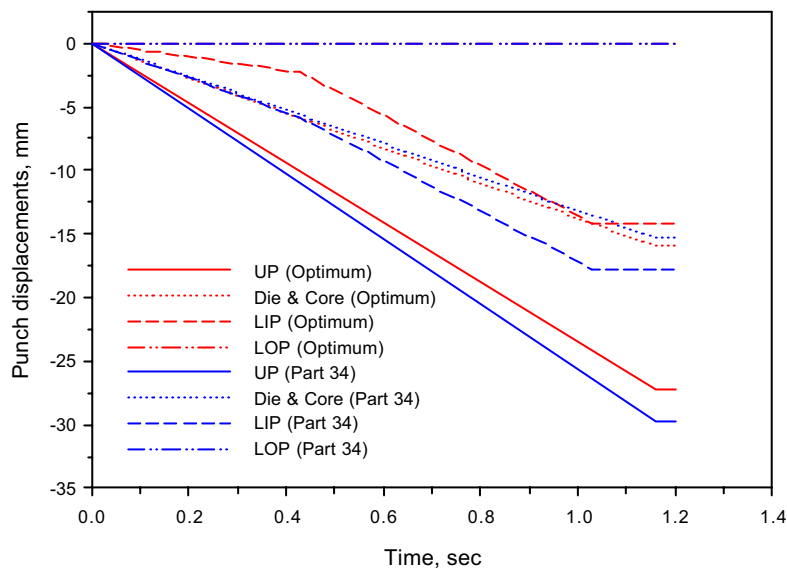


Figure 11 Comparison of loading schedule between Part 34 and optimum

Figure 12 shows the comparison of density distribution between Part 34 and optimum case, where it is clear that density distribution becomes much more uniform in optimum case. To compare quantitatively, densities in 5 blocks as defined in Figure 7 were compared. Table 4 shows this comparison. In case of Part 34 the maximum difference of density was 0.18, while in case of optimum the maximum difference was reduced to just 0.07. From these comparisons, it can be said that the optimization tool succeeded in obtaining the uniform density distribution.

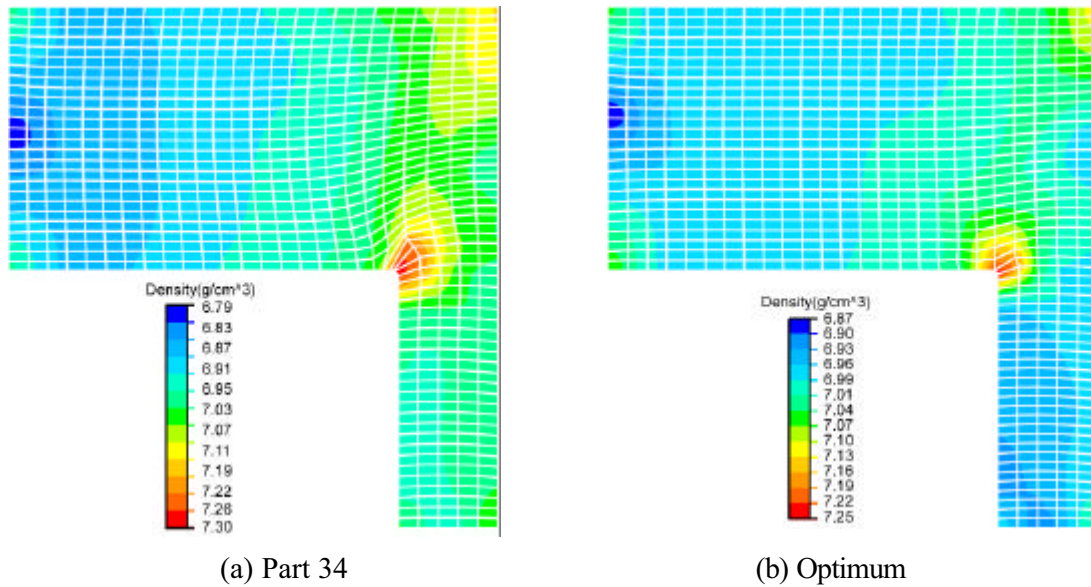


Figure 12 Comparison of density distribution between Part 34 and optimum

Table 4. Comparison of densities between Part 34 and optimal loading schedule

Block	Part 34	
	Part 34 Simulation	Optimization Simulation
1	6.89	6.97
2	6.94	6.98
3	7.07	7.02
4	7.03	6.96
5	7.00	6.95
Max. Density difference	0.18	0.07

Figure 13 shows the comparison of FSL between Part 34 and optimum case, where optimum case shows relatively small magnitude of FSL. This means that the possibility of crack formation in optimum case is lower than in Part 34. In this case the object function for optimization was the uniformity of density distribution and this result show that the efforts to minimize the density gradient can reduce the possibility of crack formation.

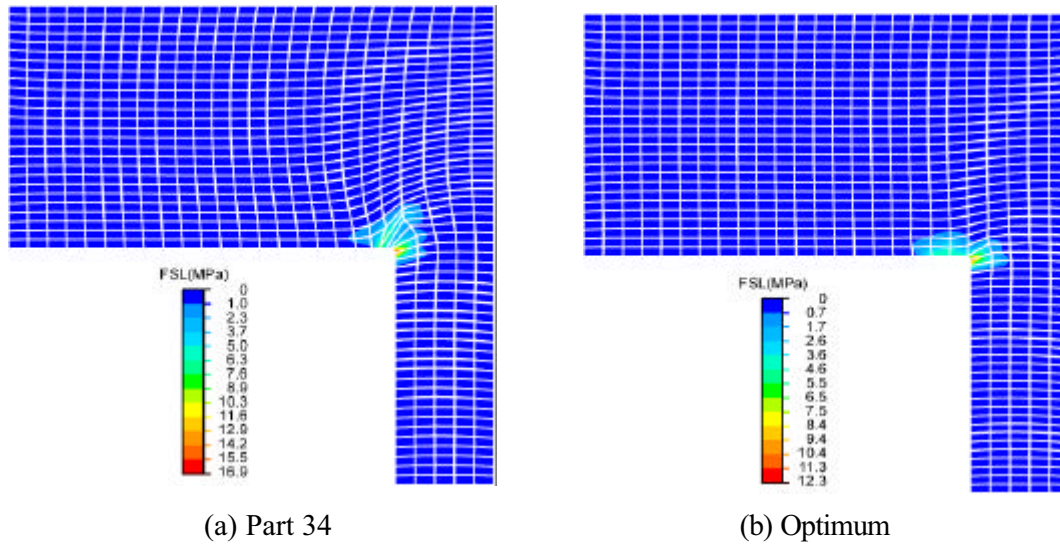


Figure 13 Comparison of failure separation length (FSL) between Part 34 and optimum

CONCLUSION

An analysis and optimization tool for die compaction process (PMsolver) was developed and applied to a practical problem. A new concept for crack formation and simple method to determine the material parameters for Shima and Oyane model were proposed. The finite element simulation results from PMsolver with the proposed crack formation and method to determine the material parameters were verified by comparing it with experiment data.

It is very important to select proper loading schedule in die compaction. The optimization scheme was applied to obtain uniform density distribution during die compaction process, where the objective function was the deviation of density and the design parameters were the loading schedule of the tools. The simulation results from the optimized loading schedule show remarkably improved the uniformity of density distribution and reduce the possibility of crack formation.

ACKNOWLEDGEMENTS

This research was sponsored by the National Science Foundation via Research Grant No. DMI-0200554.

REFERENCE

1. German, R.M. *Powder Metallurgy Science*, Metal Powder Industries Federation, Princeton, NJ, 1994.
2. PM Modnet Computer Modeling Group, "Comparison of computer models representing powder compaction process", *Powder Metall.*, Vol. 42, No. 4, 1999, pp. 301-311.

3. Kergadallan, J., Puente, G., Doremus, P. and Pavier, E. "Compression of an Axisymmetric Part with an Instrumented Press", Proc. Int. Workshop on 'Modeling of metal powder forming processes', Grenoble, France, 1997, pp. 277-285.
4. Kwon, Y.S., Chung, S.H., Binet, C.B., Zhang, R., Engel, R.S., Salamon, N.J. and German, R.M. "Application of Optimization Technique in the Powder Compaction and Sintering Process", *PM2TEC 2002*, Orlando.
5. Shima, S. and Oyane, M. "Plasticity Theory for Porous Metals", *Int. J. Mech. Sci.*, Vol. 18, 1976, pp. 33-50.
6. Doraivelu, S.M., Gegeļ, H.L., Gunasekera, J.S. and Morgan, J.T. "A New Yield Function for Compressible P/M Materials", *Int. J. Mech. Sci.*, Vol. 26, 1984, pp.527-535.
7. Kwon, Y.S., Lee, H.T. and Kim, K.T. "Analysis for Cold Die Compaction of Stainless-Steel Powder", *ASME J. Engineering Materials and Technology*, Vol. 119, 1997, pp. 366-373.
8. Coube, O. "Modeling and numerical simulation of powder die compaction with consideration of cracking", PhD Thesis, University Pierre et Marie Curie, Paris, 1998.